

Bainite Formation in a Carbon-Free Fe–Cr–N System



PHILIP KÖNIG , JONATHAN LENTZ , and SEBASTIAN WEBER

In order to promote the understanding of bainitic transformation in nitrogen alloyed steels, the microstructure, transformation kinetics, and diffusion/precipitation characteristics of an isothermally heat-treated carbon-free system Fe–5Cr–N were investigated. Quenching dilatometry was used to perform heat treatments at temperatures between 400 °C and 500 °C and simultaneously receive information about the transformation kinetics. Scanning electron microscopy (SEM) and electron backscatter diffraction (EBSD) investigations indicate a plate-to-lenticular-like, fully ferritic microstructure with nanometer scale CrN. In order to analyze the diffusion and precipitation behavior of nitrogen, atom probe tomography measurements were performed. On the one hand, nitrogen segregation was found, and on the other hand, the presence of CrN precipitates and preliminary stages of CrN nitrides were validated.

<https://doi.org/10.1007/s11661-024-07365-0>
© The Author(s) 2024

I. INTRODUCTION

IN the context of bainitic transformation in carbon (C) steels, there are many studies concerning the transformation kinetics, emerging microstructures, and the mechanisms of carbide formation, directly related to the diffusion ability of C during the bainite reaction. In contrast, there is just a small number of publications addressing the isothermal decomposition behavior of nitrogen (N) alloyed Fe-base systems which are heat treated within the temperature interval providing the conditions of para-equilibria.^[1–6] It has been shown that isothermal heat treatments of an austenitic binary Fe–2.6N system below 500 °C result in a microstructure which contains very fine acicular aggregates of ferrite and Fe₄N precipitates with high similarity to the well-investigated upper bainite in carbon steels which is distinguished by aggregates of ferrite and Fe₃C.^[1] Isothermal annealing temperatures above 500 °C, on the other hand, lead to a lamellar structure of ferrite and Fe₄N, which is described as “braunite.” Braunite possesses a significantly lower dislocation density and is discussed as the counterpart of reconstructively formed pearlite in carbon steels.^[1] At present, the transformation process of the isothermal austenite

decomposition of Fe–N systems below 500 °C is not yet sufficiently understood. There are different assumptions about the formation chronology of ferrite and Fe₄N. Foct *et al.* assume a two-stage mechanism starting with the precipitation of Fe₄N followed by the diffusionless formation of N-supersaturated plate-like ferrite from the N-depleted austenite.^[6] On the contrary, Jiang *et al.* performed in situ XRD measurements during isothermal heat treatment at 225 °C of the austenitic Fe–2.51N system and reported that ferrite is the first forming phase followed by Fe₄N.^[3] Teixeira *et al.*^[7] investigated the microstructure and kinetics of a C + N enriched low-alloy steel. It was shown that the C + N variant of the steel exhibits accelerated bainite formation compared to the N-free variant. This is attributed to the formation of CrN nitrides, which serve as nucleation sites for bainitic ferrite. In addition, a finer bainitic ferrite microstructure has been reported in the carbonitrided variant. The latter is of special interest with regard to technical applications, since the size of the sub-units in the context of bainitic steels directly influences the mechanical properties.^[8]

The limited number of studies in this area has mainly focused on the isothermal heat treatment of binary Fe–N systems with high N concentrations above 2 wt pct, leading to thermodynamic stabilization of austenite below room temperature. This inhibits direct transferability to conventional isothermal bainitization in carbon steels, which involves austenitization at elevated temperatures followed by quenching to the isothermal annealing temperature. In addition, the influence of further substitutional elements has so far only been examined briefly. In terms of steel alloying with nitrogen, it has been shown that nitrogen dissolved in the

PHILIP KÖNIG, JONATHAN LENTZ, and SEBASTIAN WEBER is with the Chair of Materials Technology, Institute for Materials, Ruhr-Universität Bochum, Universitätsstraße 150, 44801 Bochum, Germany. Contact e-mail: philip.koenig@rub.de

Manuscript submitted September 12, 2023; accepted February 22, 2024.

Article published online March 13, 2024

iron lattice may exert a beneficial influence on properties such as corrosion resistance, ductility, and strength.^[9,10] In this context, chromium (Cr) is a suitable substitutional alloying element that increases N-solubility in the Fe lattice and further enhances corrosion resistance.^[9,11] Thus, the consideration of nitrogen combined with chromium in the context of bainitic transformation also gains potential from a technological perspective.

Various research questions need to be addressed. First, it is essential to investigate whether bainitic transformation is possible in carbon-free systems with moderate N contents, leading to thermodynamically unstable austenite at room temperature. In this regard, the microstructure must be examined cooperatively with the kinetics. Since the bainitic transformation in carbon steels is significantly affected by the diffusion and precipitation characteristics of interstitially dissolved C atoms, substituting C with N may have a considerable impact on transformation kinetics and associated microstructure formation. Therefore, it is crucial to investigate the diffusion behavior of N to verify whether C and N atoms fundamentally follow a similar mechanism during the bainitic transformation.

Thus, a C-free ternary Fe–Cr–N model alloy was developed on the basis of thermodynamic calculations with the aim to investigate the isolated influence of moderate nitrogen contents below 0.3 wt pct on the bainitic transformation while allowing for comparability to the bainite transformation in carbon steels in terms of austenite stability. This comprehensive investigation of the isothermally heat-treated Fe–Cr–N system is based on dilatometry, SEM, EBSD, and APT analysis.

II. EXPERIMENTAL DETAILS

A. Selection and Production of Model Alloys

Thermodynamic equilibrium calculations were conducted using Thermo-Calc© software (Version 2021a, TCFE 10) to evaluate a suitable Fe-based model alloy with increased N-solubility, while maintaining low complexity in order to minimize interaction effects between the alloying elements. Since Cr increases the nitrogen solubility in Fe, it was utilized to achieve higher N-solution contents in the austenite.^[9] In the course of these calculations, the following phases have been included: BCC_A2 (α), FCC_A1 (γ), FCC_A1#2 (MC, MN, M(C,N)), HCP_A3 (M_2N), HCP_A3#2 (M_3N), FE4N_L1PRIME (Fe_4N , γ'), GAS, and LIQUID. As a result, a ternary Fe–Cr–N phase diagram representing the parameters in the dilatometer at 1000 °C and a pressure of 100 kPa has been created (Figure 1).

To maintain N dissolved in the material, a Cr content of 5 wt pct was chosen, as Cr-nitrides of the type CrN are thermodynamically stabilized above approximately 7.5 wt pct Cr. Since nitrogen solubility in the molten state is significantly lower than in the austenitic structure, the binary Fe–5Cr system was initially cast using vacuum induction melting from electrolytic iron and ferro-chromium in 200 g batches. Subsequently, the

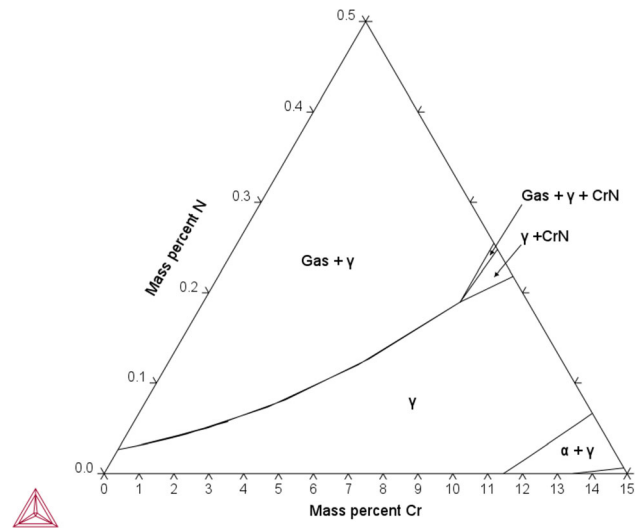


Fig. 1—Calculated ternary Fe–Cr–N phase diagram (1000 °C, 100 kPa) using the software Thermo-Calc©.

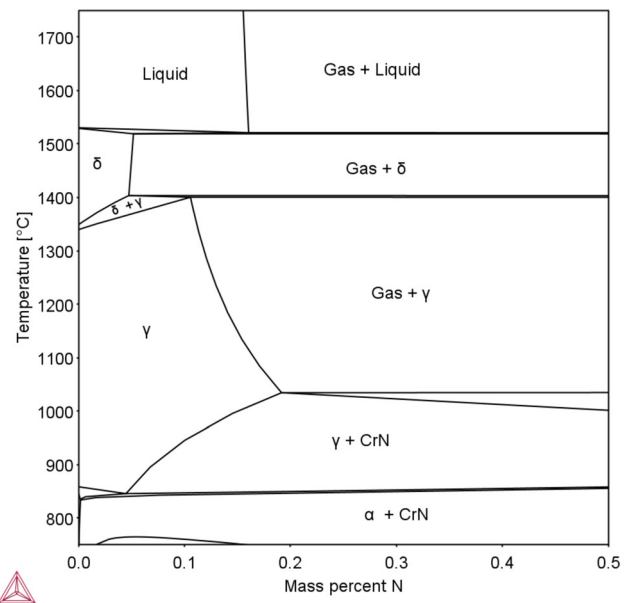


Fig. 2—Calculated phase diagram of the system Fe–4.85Cr with variable N content and a pressure of 460 kPa using the software Thermo-Calc©.

alloying process with N was realized through pressure-supported high-temperature solution annealing (HTSA). Using thermodynamic calculations, HTSA was conducted in the homogeneous austenite phase field under an N_2 atmosphere at a pressure of 460 kPa in a tube furnace, which equals the highest possible pressure. In order to prevent nitride formation, the annealing temperature has been increased to 1100 °C for 5 hours with the aim of preventing nitride formation (see Figure 2).

B. Sample Preparation

For the HTSA procedure, cylindrical specimens with a diameter of 4 mm, a length of 10 mm, and a wall thickness of 200 to 400 μm were manufactured by wire-cut electrical discharge machining from the 200 g laboratory melts. The thin-walled tubular geometry was chosen to increase the surface-to-volume ratio and decrease the diffusion distance, ensuring a homogeneous and throughout N distribution. Following HTSA, the specimens were immediately quenched in water in order to prevent precipitation of nitrides at lower temperatures. The chemical composition was subsequently validated by optical emission spectrometry (OES). Carrier gas hot extraction (CGHE) was conducted to quantify the N content in different heat treatment states. Additionally, wavelength-dispersive X-ray spectrometry (WDS) measurements were carried out for the local determination of the N concentration in the bainitized condition (Table I).

C. Dilatometry

Dilatometer experiments were conducted using a DIL805 from Bähr Thermoanalyse GmbH in quenching mode to measure austenite-to-bainite transformation-dependent length changes. The dilatometer utilized has an induction coil built-in, which enables sample heating. A thermocouple welded directly to the sample allows precise temperature measurement and simultaneously serves as a control variable for the energy input of the induction coil. Cooling is achieved through gas supply lines, which enable parallel cooling from both inside and outside for hollow-manufactured specimens. In this work, the thin-walled tubular geometry allowed quenching rates of up to $-200\text{ }^\circ\text{C/s}$.

To estimate a suitable temperature interval, the empirical approaches according to Andrews *et al.*^[12] (M_S -temperature) and Leach *et al.*^[13] (B_S -temperature) were employed to determine the lower (M_S) and upper (B_S) temperature limits for isothermal heat treatment.

$$M_S(^{\circ}\text{C}) = 539 - 423\text{C} - 30.4\text{Mn} - 12.1\text{Cr} - 7.5\text{Mo} - 17.7\text{Ni} \quad [1]$$

$$B_S(^{\circ}\text{C}) = 850 - 206\text{C} - 78\text{Mn} - 33\text{Ni} - 70\text{Cr} - 75\text{Mo} - 61\text{Si} \quad [2]$$

Due to the high comparability of interstitially dissolved N and C in the context of the austenite stabilizing effect in Fe, C has been substituted by N for the

calculation of B_S and M_S with equivalent weighting.^[9,10] The equivalent consideration of N and C for the determination of the M_S -temperature is also described in the literature and was in first approximation extended to B_S -temperature in this work.^[14] The results were determined to be approximately $400\text{ }^\circ\text{C}$ for M_S and $475\text{ }^\circ\text{C}$ for B_S , so a reasonable isothermal annealing interval from $400\text{ }^\circ\text{C}$ to $500\text{ }^\circ\text{C}$ was chosen. After a preliminary evacuation to a pressure of $4 \times 10^{-5}\text{ MPa}$, the first temperature level was carried out at $100\text{ }^\circ\text{C}$ for 2 minutes with the aim of reducing residual moisture on the surface of the specimen as well as in the environment ($\dot{T}_{0\text{ to }100\text{ }^\circ\text{C}} = 3\text{ K/s}$). Nearby the termination of this segment and the start of heating at $\dot{T}_{100\text{ to }1000\text{ }^\circ\text{C}} = 10\text{ K/s}$, the process chamber was flooded with N_2 up to a pressure of approximately 90 kPa to inhibit outgassing. After austenitization at a temperature of $1000\text{ }^\circ\text{C}$ for 10 minutes, the N-enriched specimens were quenched within 3 seconds to the respective isothermal annealing temperatures of $400\text{ }^\circ\text{C}$, $425\text{ }^\circ\text{C}$, $450\text{ }^\circ\text{C}$, $475\text{ }^\circ\text{C}$ and $500\text{ }^\circ\text{C}$. The isothermal temperatures were held for 60 minutes. The quenching rate of the sample heat treated at $450\text{ }^\circ\text{C}$ was $\dot{T}_{1000\text{ to }450\text{ }^\circ\text{C}} = -183.3\text{ K/s}$. Finally, quenching to room temperature was performed ($\dot{T}_{450\text{ to }20\text{ }^\circ\text{C}} = -85\text{ K/s}$). Figure 3 schematically illustrates the temperature profiles applied to the samples with the aim of bainitization.

D. Hardness Testing

The Vickers hardness tests were performed using an automated testing device, the KB30S by KB Prüftechnik GmbH located in Hochdorf-Assenheim, Germany. The tests were conducted in accordance with DIN EN ISO 6507-1^[15] to accurately assess the hardness of the samples. Each measurement involved applying a testing force of 4903 N (HV0.5), and a total of five measurements were taken.

E. Microscopy

The microscopic examinations were performed with an emphasis on the developed microstructure and in particular the phases present. The SEM device MIRA 3 from TESCAN equipped with EBSD and wavelength-dispersive x-ray spectrometry (WDS) from Oxford Instruments was used for the microstructure investigation of the isothermally heat-treated samples. The considered specimens were embedded in electrically conductive resin. After grinding (mesh sizes: 320, 500, 1000, 2500) subsequent polishing (diamond particle sizes: $6\text{ }\mu\text{m}$, $3\text{ }\mu\text{m}$, $1\text{ }\mu\text{m}$, oxide polishing suspension $0.25\text{ }\mu\text{m Al}_2\text{O}_3$) without etching was performed. SEM images were taken with an accelerating voltage of 20 kV

Table I. Chemical Composition of the Used Material in the Initial State (Prior to Nitriding) Measured by OES

State	C	N	Cr	Ni	Mo	Mn	Si	P	S	Fe
Initial Steel	0.001	0.007	4.845	0.003	0.004	0.008	0.001	0.001	0.002	balance

and a working distance of 6.5 mm in backscatter electron (BSE) contrast. The EBSD investigations were also performed with an accelerating voltage of 20 kV and a working distance of 17 mm to specimens tilted by 70 deg. The detector distance from the specimen was approximately 5 mm. In order to analyze the collected data, the software Aztec from Oxford Instruments was used.

F. Atom Probe Tomography

In order to investigate the precipitation as well as diffusion behavior of N, atom probe tomography was applied. This allows the combinatorial three-dimensional investigation of local chemical composition down to atomic resolution, providing a unique opportunity to investigate the solution state and diffusion behavior of individual elements. APT samples were fabricated according to the procedures presented in Reference 16 with the aim to lift out sub-unit interface volumes. Figure 4 shows an SEM image of the extracted volume of the sample bainitized at 450 °C before the sharpening process. Individual sub-units can be recognized, which is of great importance for the research objective as well as for the interpretation of the APT result.

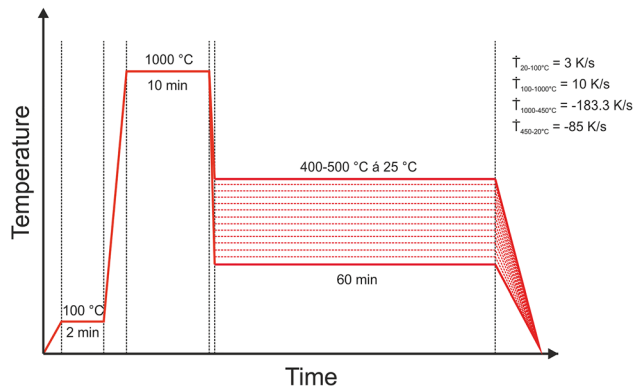


Fig. 3—Schematic time temperature profiles used in the dilatometer.

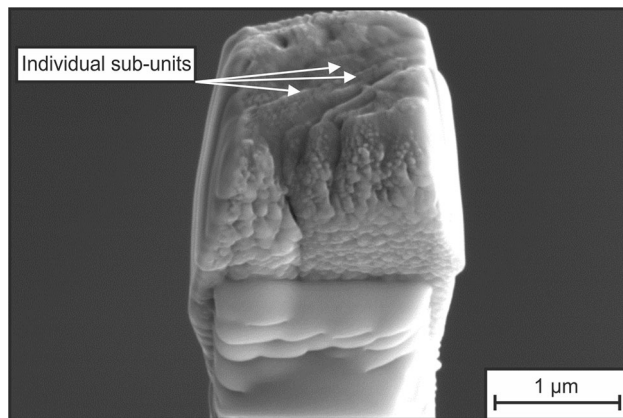


Fig. 4—SEM image of the APT sample isothermally annealed at 450 °C before the sharpening process in the FIB.

The dual-beam focused ion beam (FIB) system FEI Helios G4CX was used for this purpose. For the APT measurements, the equipment LEAP 5000 XR of the manufacturer Cameca Instruments was used in pulsed voltage mode at 70 K with a pulse fraction of 20 pct and a pulse repetition rate of 0.075 atoms per pulse. Finally, the raw data were analyzed using the software AP Suite 6 from Cameca.

III. RESULTS AND DISCUSSION

A. Material and HTSA

The N and O concentrations measured by CGHE and WDS are listed in Table II. The HTSA procedure resulted in a total N content of 0.192 wt pct which is approximately the calculated nitrogen solubility in the austenite at 1100 °C and 460 kPa (compare Figure 2). In the course of the HTSA process also, the oxygen (O) concentration increased to 0.194 wt pct. Since a brittle oxide layer was formed on the sample surface during the HTSA, the significant increase in O level is due to the measurement of the surface oxide layer and not to O uptake by the base material. Thus, no O could be detected in the bainitized samples after metallographic preparation.

Since the N concentration calculated by Thermo-Calc and that determined by CGHE are almost identical (see Figure 2), a suitable process for alloying with N in low to medium contents was found with the aid of the applied pressure-assisted HTSA process. Further N uptake from the process atmosphere during bainitization is evident by the N content of 0.24 wt pct after. This is identical for all samples, regardless of the isothermal temperature. The system under consideration is therefore titled Fe-5Cr-0.2N as follows.

The N level of approximately 0.2 wt pct used in this study is well below the N levels used in the few published studies on the effect of N during bainitization.^[1-4,6] This condition was an important consideration in the design of this study. Contrary to the literature, the lower N content realized here does not lead to a stabilization of the austenite below RT, so that a transformation of the face-centered cubic (fcc) to body-centered cubic (bcc) lattice of the iron matrix phase would occur upon cooling of the samples after austenitization, even without the precipitation of nitrides. At the high N contents used in the literature, bainitization is discussed as being possible only through the precipitation of nitrides, the resulting N depletion of the matrix and the consequent destabilization of the austenite.

B. Dilatometry and Hardness Testing

The relative length change of the isothermal segment and hardness as a function of isothermal temperature is shown in Figure 5.

The specimens with T_{iso} of 400 °C and 425 °C show a slight linear decrease in length after reaching the isothermal temperature. In the context of isothermal heat treatments of carbon steels, this behavior is

associated with the formation of carbides. The precipitation of nitrides with a comparable effect could be possible in the system considered here. Since no length expansion takes place during the isothermal holding stage, a prior phase transformation during cooling is conceivable. To address this concern, one sample was quenched directly to room temperature after austenitization at 1000 °C. The corresponding length change profile during the cooling interval is shown in Figure 6.

Accordingly, a linear expansion can be observed during cooling, which is attributed to the martensitic transformation. The dashed lines mark the beginning of the expansion, which corresponds to the M_S temperature. As $M_S = 443.1$ °C is above the isothermal holding levels $T_{iso} = 425$ °C and $T_{iso} = 400$ °C, a previous martensitic transformation explains the absence of expansion during the isothermal holding phase. In

Table II. N- and O-Concentrations of the Fe–4.85Cr–0.192N (Respectively Fe–4.85Cr–0.24N) System After Pressure Supported HTSA (1100 °C, 460 kPa, 5 h) Measured by CGHE and N-Concentrations After the Isothermal Heat Treatment at $T = 450$ °C for 1 h Measured by WDS

State	N	O
After HTSA	0.192 ± 0.04	0.194 ± 0.043
After Isothermal Treatment	0.240 ± 0.02	—

Values are given in wt pct.

contrast, the samples with higher T_{iso} show expansion during isothermal treatment. This behavior is well described in the literature and is typically caused by the transformation from the closer packed fcc austenite to the bainitic bcc lattice.^[8] When considering the time, an influence of the isothermal temperature on the expansion profile can also be seen. Accordingly, higher temperatures lead to an earlier attainment of a horizontal curve and thus to a shorter expansion interval. While for $T_{iso} = 500$ °C the expansion is completed shortly

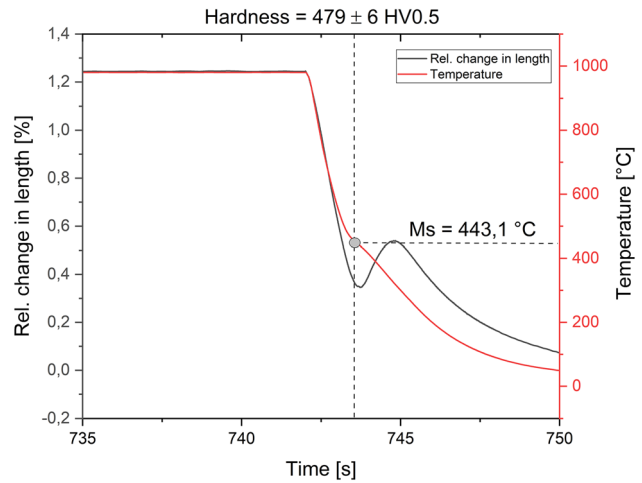


Fig. 6—Relative length change and temperature profile during quenching, recorded in situ by dilatometry and hardness after quenching to room temperature. The dashed line marks the start of the martensitic transformation.

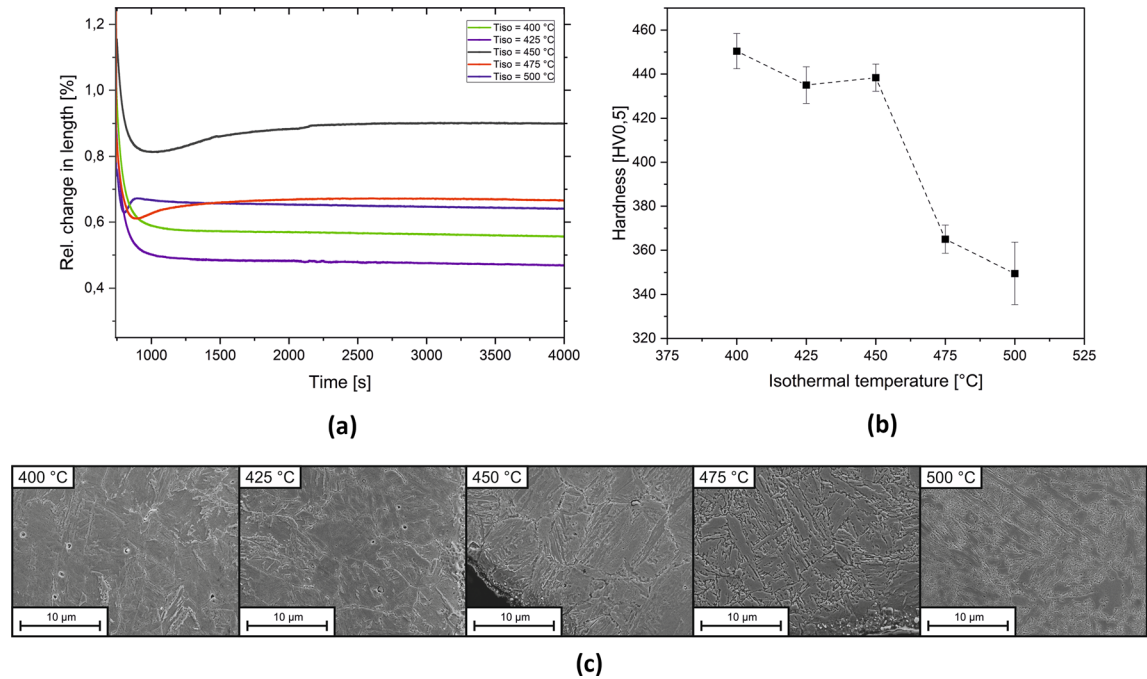


Fig. 5—Relative length change during isothermal heat treatment, recorded in situ by dilatometry (a). Hardness as a function of the isothermal annealing temperature (b) with corresponding SEM images (c).

after reaching the isothermal holding stage, at $T_{\text{iso}} = 450\text{ }^{\circ}\text{C}$ a significantly longer expansion interval occurs which leads to a horizontal profile at about $t = 3000$ seconds. Since in the context of isothermal phase transformations the reaching of an horizontal curve is considered as the end of transformation, a higher transformation temperature in the contemplated Fe–5Cr–0.2N system seems to induce an acceleration of the phase transformation.^[8,17] The relative length change has increased by about 0.1 pct in this interval. The overlap of possible precipitation processes with the transformation of fcc to bcc crystal lattices cannot be excluded, so that the relative length change associated with the bainite formation could be larger.^[8,17] In the context of bainitic transformations by isothermal heat treatments in C-steels, common relative length changes below 1 pct are discussed. Thus, the basic transformation behavior seems similar to the bainitic transformation in C-bainites. With regard to the hardness, a drop of about 80 HV 0.05 can be observed with increasing temperature between $T_{\text{iso}} = 450\text{ }^{\circ}\text{C}$ and $T_{\text{iso}} = 475\text{ }^{\circ}\text{C}$ (see Figure 5). The reason for this could be based on two hypotheses. Either the reason for the decrease in hardness is the bainite transformation temperature itself, as lower temperatures lead to a greater formation of bainitic ferrite, which has a lower thickness and is therefore harder than bainitic ferrite formed at higher temperatures, at which a change in the transformation mechanism is not to be expected.^[8] Or a change in the transformation mechanism could be a cause of the decrease in hardness. According to the calculation using equation 2.2, the B_S -temperature is approximately $475\text{ }^{\circ}\text{C}$. Thus, a transition from a displacive to a reconstructive transformation above $T_{\text{iso}} = 450\text{ }^{\circ}\text{C}$ is also conceivable, which has a decisive influence on the resulting hardness. When observing the overview micrographs in Figure 5, a change in the microstructure morphology is also recognizable between $T_{\text{iso}} = 450\text{ }^{\circ}\text{C}$ and $T_{\text{iso}} = 475\text{ }^{\circ}\text{C}$. For example, the sample with $T_{\text{iso}} = 450$ shows a predominantly plate-shaped microstructure, which is much finer in appearance than the samples with a higher T_{iso} . In addition, the microstructure components of the sample with $T_{\text{iso}} = 475\text{ }^{\circ}\text{C}$ are considerably rounder in shape, which also indicates a reconstructive transformation.^[8] Nakada *et al.*^[1] reported a transition temperature between $480\text{ }^{\circ}\text{C}$ and $550\text{ }^{\circ}\text{C}$ in the framework of isothermal decomposition studies of Fe–N systems and justified this with a change of the morphology and significant decrease of the dislocation density. The latter has a considerable influence on the mechanical properties and could explain the drop in hardness above $T_{\text{iso}} = 450\text{ }^{\circ}\text{C}$ that occurs in this study. At 479 ± 6 HV0.05, the hardness of the martensitic sample shown in Figure 6 is slightly higher than the T_{iso} samples of $400\text{ }^{\circ}\text{C}$ and $425\text{ }^{\circ}\text{C}$, which are also assumed to be martensitic. This behavior is well known and can be explained by tempering effects that the isothermally heat-treated samples have experienced. As a result, the tetragonal distortion of the crystal lattice is reduced, which leads to a reduction in hardness.^[18,19]

The sample treated at $T_{\text{iso}} = 450\text{ }^{\circ}\text{C}$ shows the largest relative change in length of all the experiments performed and the curve profile, with its decreasing slope as time progresses, resembles the bainitic transformation behavior of conventional carbon steels.

Therefore, the sample with an isothermal heat treatment at a temperature of $T_{\text{iso}} = 450\text{ }^{\circ}\text{C}$ was selected in order to investigate the microstructure, the diffusion, and precipitation characteristics within the context of bainitic nitrogen-containing carbon-free Fe-based alloys.

C. Microstructure, Phase Analysis, and Diffusion Characteristics

SEM images of the microstructure of the sample isothermally heat treated at $450\text{ }^{\circ}\text{C}$ are shown in Figure 7.

Figure 7(a) shows an overview of a predominantly plate-like structure that forms in packets of many thin plates with the same orientation. In Figure 7(b), individual sub-units can be seen, some of which follow a lath-like to lenticular shape. The width of the sub-units varies from about 100 to 400 nm. The length is about 5 to $10\text{ }\mu\text{m}$. A comparison of Figure 7(b) with the microstructure of carbide-free bainite with medium carbon content shows a high morphological similarity to upper bainite.^[8,20] This is characterized by bundles of ferritic sub-units with similar orientation.^[8,21] The combination of isothermal transformation and the plate-like to lenticular shape of the sub-units, which are also arranged in a bundle with similar orientation, suggests the formation of N-bainite. Regions of retained austenite stabilized by C enrichment and/or carbides are usually present between individual sub-units of upper C-bainites.^[8,22] Furuhashi *et al.* investigated the crystallography and microstructure of upper bainite in Fe–9Ni–(0.15–0.5)C alloys after different heat treatments. After annealing at $400\text{ }^{\circ}\text{C}$, a microstructure of bainite laths and retained austenite was formed in the low C variant. The morphology of individual bainite sub-units appears to be comparable to the microstructure present in this study.^[23] According to both the continuous and discontinuous approaches to bainite transformation, carbide precipitation has a significant effect on the assembly of phase fractions by reducing local austenite stability and thus increasing the driving force for further ferrite formation.^[21,24,25] Since dissolved N atoms lead to a stabilization of the fcc lattice analogous to C, a similar behavior can be assumed in the context of N-bainites. Accordingly, EBSD studies were performed to validate the precipitation of nitrides and to determine potential retained austenitic fractions.

In Figure 8(a), an EBSD image of the Fe–5Cr–0.2N sample after isothermal heat treatment at $450\text{ }^{\circ}\text{C}$ can be seen. According to the EBSD analysis, a completely bcc microstructure was obtained after the isothermal heat treatment for 1 hour. In addition, CrN nitrides have been indicated, which are increasingly present in linear form (Figure 8(b)). This supports the assumption that the precipitation of nitrides in the context of bainitic transformation proceeds in a similar manner and even

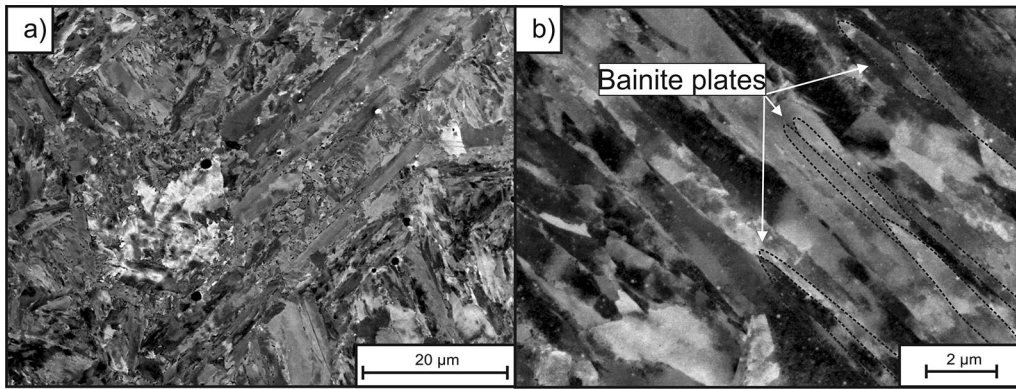


Fig. 7—Overview (a) and detail (b) SEM images of the Fe-5Cr-0.2N sample after isothermal heat treatment at 450 °C with indication of some individual bainite plates in (b).

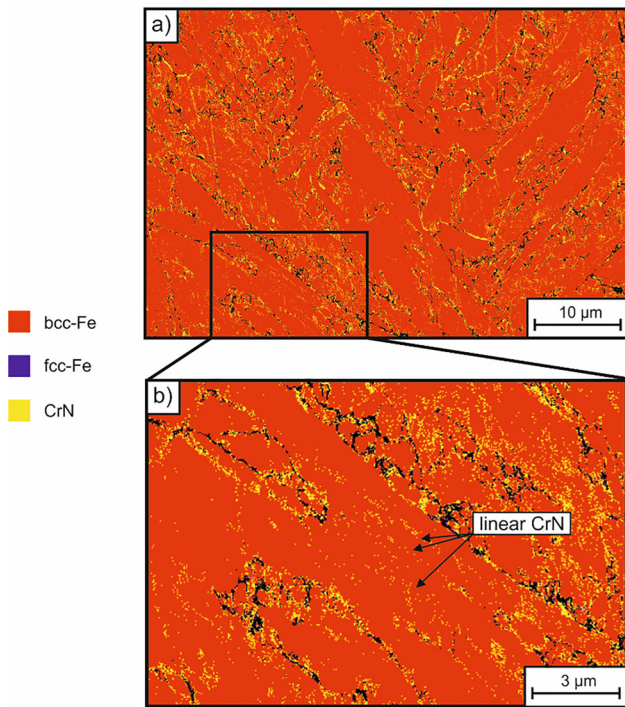


Fig. 8—Overview (a) and detail (b) EBSD images of the Fe-5Cr-0.2N sample after isothermal heat treatment at 450 °C in different resolutions.

generates largely similar thermodynamic conditions compared to carbide precipitation in C-bainites. In previous works on the bainitization of binary Fe-N systems with N concentrations of about 2 wt pct, fully bainitic microstructures were also observed after isothermal heat treatments.^[1-4,6] However, Fe₄N nitrides have been detected between individual ferrite plates, which are discussed as the counterpart of Fe₃C in upper C-bainites. The presence of Fe₄N nitrides could not be observed in this study.

In order to validate the presence of CrN nitrides and to study the solution state/location, segregation, and diffusion behavior of N on the nanoscopic scale, APT investigations were carried out. An APT sample was taken between sub-units on which increased Cr-nitrides

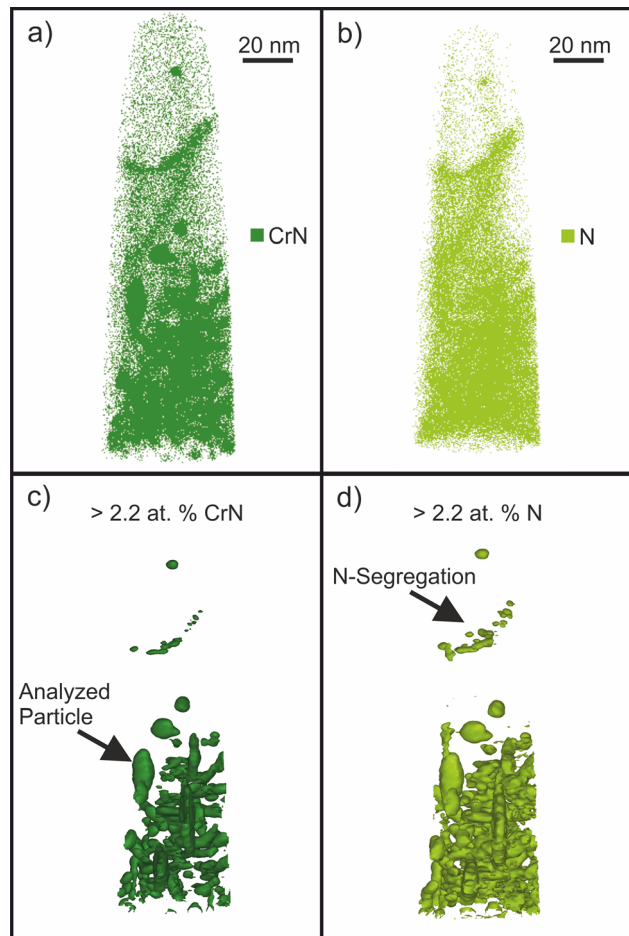


Fig. 9—(a) CrN and (b) N atom map of the specimen isothermally heat-treated at 450 °C for 1 h. (c) and (d), respectively, show the corresponding isoconcentration surfaces with a threshold of 2.2 at. pct.

were detected according to the EBSD studies (see Figure 4). In particular, the nanoscopic segregation behavior of N represents an essential aspect in understanding the bainitic transformation in N alloyed steels and has so far been studied only indirectly on the basis of precipitation behavior of various nitrides. The results

of the APT- measurements are shown in Figure 9. The subimages (a) and (b) display the CrN and N atom maps of the isothermally heat-treated Fe–5Cr–0.2N sample at 450 °C. Figures 9(c) and (d) represent the isoconcentration surfaces of N and CrN with a limit value of 2.2 at. pct in order to emphasize the segregation and precipitation geometry. Accordingly, only the areas that are above the specified limit are highlighted.

The CrN atom map reveals particles with predominantly spherical to ellipsoidal morphology and a size of up to about 20 nm in length. In order to investigate the stoichiometry of the detected particles in detail, a concentration profile (Figure 10) has been plotted with respect to the particle labeled in Figure 9(c).

The center of the particle under consideration is found approximately at a distance of 25 nm and reveals a width of about 10 nm. While the matrix contains about 95 at. pct Fe, Figure 10 shows that in the particle interior about 50 at. pct Cr and 50 at. pct N are present. Thus, the assumption of CrN precipitation is strongly supported.

The detected CrN nitrides seem to follow different arrangements. On the one hand, they are more prevalent in the lower segment of the observed tip volume. On the other hand, they are arranged similar to a curved plane, indicating the presence of an interface in the upper segment. In addition, the latter show significantly smaller dimensions with a size below 5 nm. This leads to the assumption that their formation is subject to varying conditions. In the context of nanostructured carbon bainites, Timokhina *et al.*^[26] demonstrated, also on the basis of APT investigations, the formation of cementite particles with dimensions of about 10 nm, which grow according to a para-equilibrium mechanism. In contrast to Fe₃C precipitation, the formation of CrN nitrides requires both Cr and N diffusion. Bhadeshia investigated the diffusivity of various elements in fcc-iron and bcc-iron. In the course of this, the diffusion length of Cr atoms in bcc-iron within 1 hour at a temperature of $T = 500$ °C is estimated to be about 10 nm.^[8] According to the definition of a

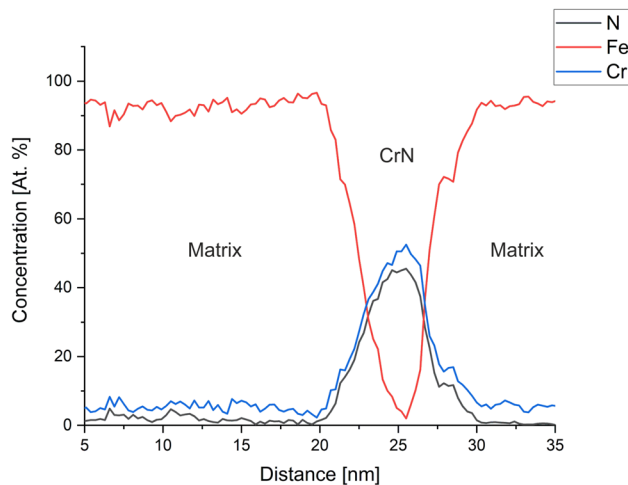


Fig. 10—Concentration profile of the analyzed particle shown in Fig. 9(c).

para-equilibrium, the CrN formation is therefore impossible. Taking the size of the formed CrN nitrides into account, the formation during the isothermal heat treatment at $T = 450$ °C appears possible.

When assuming the diffusion behavior of C during bainitization, there is still disagreement.^[27] Without taking the time into account, however, a redistribution of C in the surrounding austenite is assumed according to all transformation hypotheses which leads to a C-concentration profile with a peak close to the α - γ -interface after the bainite plate growth is finished.^[8,27,28] This behavior would also be conceivable for the scenario exemplified here, since both C and N as interstitially dissolved atoms are subject to comparable diffusivity in iron due to their similar atomic radii.^[8,9] Observing the atom maps in Figures 9(c) and (d), it is also noticeable that no precipitates occur near the interface. It would be conceivable that, to a limited extent, also Cr could diffuse to the interface, which would explain the precipitate-free region with a span of approximately 20 to 25 nm in both directions. Figure 11 shows the plotted N and Cr concentration across the suggested interface. The dashed lines mark the interface transition and indicate a significant enrichment of N up to a value of about 1.5 at. pct in an interval of about 12 to 14 nm.

Hence, analogous to C, N seems to increasingly enrich in the surrounding austenite and segregate plane-like at the α - γ -interfaces with proceeding bainite fraction. A slightly increased concentration of Cr to approx. 6 at. pct within the interface is also evident, supporting the hypothesis of Cr diffusion to the interface. The bainite formation followed by subsequent CrN precipitation, which reduces the austenite stability and allows its complete transformation into bainitic ferrite therefore appears reasonable. Caballero *et al.* investigated the redistribution of alloying elements during tempering of a nanocrystalline steel at a temperature of $T = 450$ °C by APT, also demonstrating a diffusion of Cr toward a bainite–austenite interface, which resembles with the observations in this work.^[29] The linear CrN formation observed from the EBSD studies corresponds to the

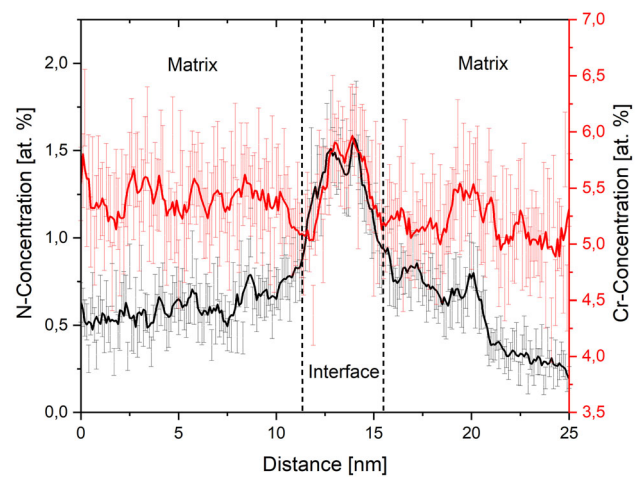


Fig. 11—Concentration profile of N and Cr across the assumed interface shown in Fig. 9(d).

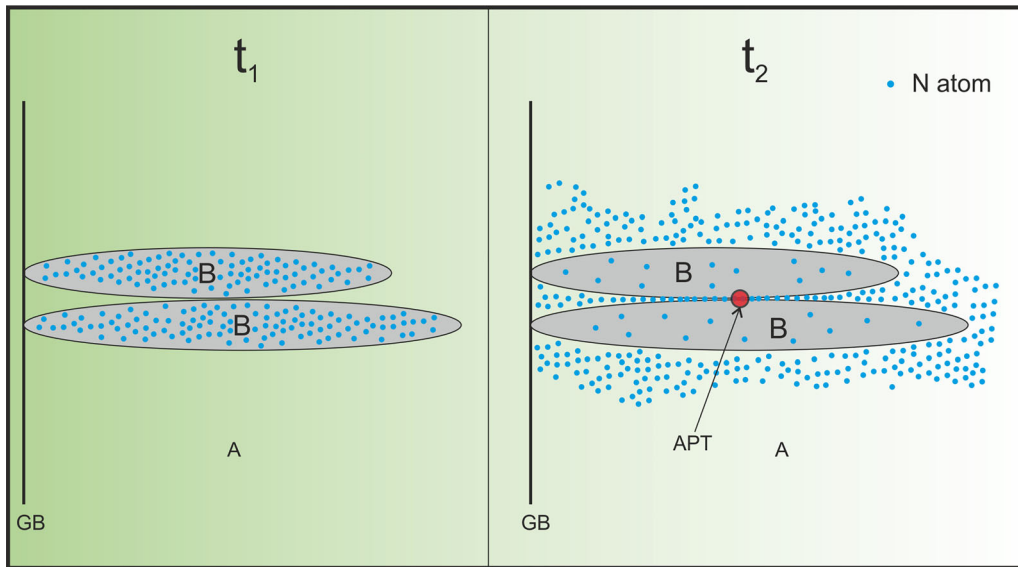


Fig. 12—Schematic illustration of the assumed diffusion characteristics of N in the context of bainite growth with indication of the possible APT volume.

APT studies and supports the theory that CrN forms likewise to Fe₃C in upper C-bainites between individual plates, but with the short-range diffusion of Cr. The similarity to the bainite in carbon steels would thus be given. Provided that the temperature is sufficiently high to allow short-range diffusion of substituted atoms, even the precipitation behavior of Fe₃C in upper carbon bainites and CrN in the investigated system appears comparable. Figure 12 shows a schematic representation of the hypothesis in which the discontinuous bainite conversion theory was assumed without considering the precipitation of nitrides.

While t_1 describes the time immediately after diffusionless growth of bainite plates, t_2 shows the considered redistribution of N atoms in the surrounding austenite, which leads to plane-like segregation effects in the region of the plate interstices. In addition, the possible investigated volume APT is shown, matching the hypothesis of plane-like N segregation between several plates.

Besides the detection of CrN nitrides and N segregation effects, the APT measurement indicates that the C-concentration appears negligible, which was the main objective of this study to allow an isolated consideration of the influence of N on the bainitic transformation.

IV. CONCLUSION AND OUTLOOK

The microstructure, transformation kinetics, and diffusion/precipitation characteristics of the isothermally heat-treated carbon-free system Fe–5Cr–0.2N were investigated by means of dilatometry, SEM, EBSD, and APT in this work.

With the applied pressure-assisted HTSA process, an almost C-free ternary Fe–5Cr–0.2N system could be realized. The dilatometrically processed heat treatment

with the aim of bainitization consisting of austenitizing at 1000 °C followed by quenching to an isothermal temperature of 450 °C revealed a relative change in length profile which is typical for bainitic transformations. SEM and EBSD examinations revealed a completely ferritic nanometer scale microstructure after an isothermal annealing time of 1 hour. The morphology appears in lath-like to lenticular aggregates which are predominantly present in bundles with similar orientation. The width of individual plates is approximately 100 to 500 nm, with the length in some cases reaching up to 5 μm. In addition, the presence of CrN nitrides was indicated by EBSD and confirmed by APT, which are mainly arranged in a linear pattern. Due to the high similarity to the microstructure of the upper bainite in C-steels combined with the isothermal transformation characteristic, the N-induced formation of bainite is assumed in this work. APT measurements could confirm the presence of small CrN nitrides with the size of 5 to 10 nm. In addition, a plane-like segregation effect was found with respect to N, which in the context of bainite transformation indicates a diffusion behavior similar to C.

The precipitation behavior of CrN nitrides in the context of bainitic transformation still appears somewhat unclear. Therefore, an investigation by means of transmission electron microscopy (TEM) should be focus of further studies. In particular, crystallographic characteristics can be determined in order to identify not only the composition but also the crystal lattice of the CrN. In the course of this, crystallographic orientation relationships should also be investigated in order to determine the parent phase of the CrN nitrides. In specific, the latter is of great significance with respect to the overall kinetics and thermodynamics of the bainitic transformation.

ACKNOWLEDGMENTS

The authors kindly acknowledge the financial support of the German Research Foundation (DFG) within the project 493947509 “Influence of an Si3N4 powder additive on the PBF-LB processability of stainless steels and the microstructure development during PBF-LB and subsequent HIP-URQ redensification,” which is part of the priority program SPP2122 “Materials for Additive Manufacturing (MATframe).”

AUTHOR CONTRIBUTIONS

P. König contributed toward conceptualization, data curation, formal analysis, investigation, methodology, validation, visualization, writing—original draft, and writing—review and editing. J. Lentz contributed toward conceptualization, methodology, supervision, writing—review and editing, and project administration. S. Weber contributed toward conceptualization, resources, supervision, writing—review and editing, project administration, and funding acquisition.

COMPETING INTERESTS

The authors declare that they have no known competing financial interests or personal relationships that could have appeared to influence the work reported in this paper.

FUNDING

Open Access funding enabled and organized by Projekt DEAL.

OPEN ACCESS

This article is licensed under a Creative Commons Attribution 4.0 International License, which permits use, sharing, adaptation, distribution and reproduction in any medium or format, as long as you give appropriate credit to the original author(s) and the source, provide a link to the Creative Commons licence, and indicate if changes were made. The images or other third party material in this article are included in the article's Creative Commons licence, unless indicated otherwise in a credit line to the material. If material is not included in the article's Creative Commons licence and your intended use is not permitted by statutory regulation or exceeds the permitted use, you will need to obtain permission directly from the copyright

holder. To view a copy of this licence, visit <http://creativecommons.org/licenses/by/4.0/>.

REFERENCES

1. N. Nakada, N. Fukuzawa, T. Tsuchiyama, S. Takaki, T. Koyano, T. Iwamoto, and Y. Omori: *ISIJ Int.*, 2013, vol. 53, pp. 139–44.
2. D. Jiao, C.P. Luo, and J. Liu: *Scripta Mater.*, 2007, vol. 56, pp. 613–16.
3. Z.-J. Jiang, X.-L. Li, J.-F. Gu, M.-J. Hu, and Z.-C. Zhu: *Surf. Coat. Technol.*, 2008, vol. 202, pp. 2638–43.
4. Z. Jiang, X. Li, J. Gu, M. Hu, and Z. Zhu: *Appl. Surf. Sci.*, 2008, vol. 254, pp. 7361–64.
5. S.D. Catteau, H.P. van Landeghem, J. Teixeira, J. Dulcy, M. Dehmas, S. Denis, A. Redjaïmia, et al.: *J. Alloys Compd.*, 2016, vol. 658, pp. 832–38.
6. J. Foct, P. Rohegude, and A. Hendry: *Acta Metall.*, 1988, vol. 1988, pp. 501–05.
7. J. Teixeira, S.D. Catteau, H.P. van Landeghem, J. Dulcy, M. Dehmas, A. Redjaïmia, S. Denis, et al.: *HTM J. Heat Treat. Mater.*, 2018, vol. 73, pp. 144–56.
8. H.K.D.H. Bhadeshia: *Bainite in Steels: Theory and Practice*, 3rd ed. CRC Press, Boca Raton, 2018.
9. V.G. Gavriljuk and H. Berns: *High Nitrogen Steels: Structure, Properties, Manufacture, Applications*, Springer, Berlin, 1999.
10. H. Berns, V. Gavriljuk, and S. Riedner: *High Interstitial Stainless Austenitic Steels*, Springer, Berlin, 2013.
11. H. Feichtinger, A. Satir-Kolorz, and Z. Xiaohong: *High Nitrogen Steel*, 1989, vol. 88, p. 75.
12. K.W. Andrews: *J. Iron Steel Inst.*, 1965, vol. 203, pp. 721–27.
13. L. Leach, Dissertation, Stockholm, 2018.
14. N. Krasokha and H. Berns: *HTM J. Heat Treat. Mater.*, 2011, vol. 66, pp. 150–64.
15. DIN EN ISO 6507-1:2018-07, *Metallische Werkstoffe - Härteprüfung nach Vickers - Teil 1: Prüfverfahren (ISO_6507-1:2018)*; Deutsche Fassung EN ISO 6507-1:2018, Berlin, Beuth Verlag GmbH, <https://doi.org/10.31030/2778746>.
16. K. Thompson, D. Lawrence, D.J. Larson, J.D. Olson, T.F. Kelly, and B. Gorman: *Ultramicroscopy*, 2007, vol. 107, pp. 131–39.
17. M.A. Santajuana, A. Eres-Castellanos, V. Ruiz-Jimenez, S. Allain, G. Geandier, F.G. Caballero, and C. Garcia-Mateo: *Metals*, 2019, vol. 9, p. 925.
18. D. Kalish and M. Cohen: *Mater. Sci. Eng.*, 1970, vol. 6, pp. 156–66.
19. H.K. Bhadeshia and R.W.K. Honeycombe: *Steels: Microstructure and Properties*, Elsevier, Oxford, 2017.
20. G. Papadimitriou and G. Fourlaris: *J. Phys. IV France*, 1997, vol. 07, pp. C5-131–36.
21. H.K.D.H. Bhadeshia and D.V. Edmonds: *MTA*, 1979, vol. 10, pp. 895–907.
22. H.I. Aaronson and C. Wells: *Trans. AIME*, 1956, vol. 8, pp. 1216–23.
23. T. Furuhashi, H. Kawata, S. Morito, and T. Maki: *Mater. Sci. Eng. A*, 2006, vol. 431, pp. 228–36.
24. S.J. Matas and R.F. Hehemann: *Trans. Metall. Soc. AIME*, 1961, vol. 221, pp. 179–85.
25. A. Hultgren: *Trans. Am. Soc. Met.*, 1947, vol. 39, pp. 915–1005.
26. I.B. Timokhina, E.V. Pereloma, S.P. Ringer, R.K. Zheng, and P.D. Hodgson: *ISIJ Int.*, 2010, vol. 50, pp. 574–82.
27. H.I. Aaronson, W.T. Reynolds, G.J. Shiflet, and G. Spanos: *MTA*, 1990, vol. 21, pp. 1343–80.
28. H.I. Aaronson and H.J. Lee: *Scripta Metall.*, 1987, vol. 21, pp. 1011–16.
29. F.G. Caballero, M.K. Miller, C. Garcia-Mateo, C. Capdevila, and S.S. Babu: *Acta Mater.*, 2008, vol. 56, pp. 188–99.

Publisher's Note Springer Nature remains neutral with regard to jurisdictional claims in published maps and institutional affiliations.